Mechanical model and verification of tillage layer compaction considering the operating dynamics of heavy tractor units

Xiao Yang[1], Hongrui Hu[1], Xianglei Liu[1], Junhao Huang[2], Wenjie Li[2*]

(1. *College of Engineering, China Agricultural University, Beijing 100083, China*;
2. *Logistics Academy, Xuzhou 221000, Jiangsu, China*)

Abstract: Plowing operations can improve the quality of the shallow soil layer, but plowing tractors still cause compaction effects on the deeper soil layers. The temporal and spatial accumulation of compaction effects can hinder crop growth, thereby reducing the overall efficiency of plowing operations and creating obstacles to soil ecological health. It is urgent to address the bottlenecks in mechanized ecological operations. This paper addresses the unclear mechanical effects of heavy-duty tractor tillage equipment on soil compaction in the tillage layer. By integrating and constructing a "heavy-duty tractor-tillage layer soil" system dynamics coupling model, it identifies the primary influencing factors of joint tillage operations on soil compaction in the tillage layer and explores the response patterns of tillage equipment parameters to the soil compaction process. The research results indicate that as the number of compaction operations increases, soil compaction increases, and soil stress transmission shows a gradually decreasing trend; when the tillage unit's operating speed is 3 km/h, the soil stress at a depth of 10 cm can reach a maximum of 499.2 kPa; when the operating speed is 6 km/h, the soil stress at a depth of 10 cm reaches a maximum of 469.1 kPa; when the operating speed is 9 km/h, the soil stress at a depth of 10 cm reaches a maximum of 438.8 kPa; when the acceleration and longitudinal acceleration increase, soil stress correspondingly increases; when the direction of lateral acceleration changes, the center of gravity of the tractor shifts, and the trends in soil stress on the inner and outer sides of the tires are opposite. The research findings can provide theoretical references for improving the operational efficiency of the unit and the development of black soil protection and utilization technologies.

Keywords: heavy-duty wheeled tractor, tillage compaction mechanism, impact of crew operations, mechanical ecology, black earth conservation

DOI: 10.25165/j.ijabe.20251805.9372

Citation: Yang X, Hu H R, Liu X L, Huang J H, Li W J. Mechanical model and verification of tillage layer compaction considering the operating dynamics of heavy tractor units. Int J Agric & Biol Eng, 2025; 18(5): 154–164.

1 Introduction

The soil is an important carrier of crop survival. Soil quality has a vital impact on crop growth and is an important guarantee for the sustainable development of agriculture in the country. One of the most important problems facing a country's cultivated land is the mechanical compaction of soil[1]. This problem is not only a huge obstacle to the development of a country's agriculture, but also a major obstacle to the sustainable development of global agriculture. Northeast China produces approximately 25% of the country's grain and ensures national food security; however, with the promotion and application of agricultural machinery, the Northeast region is facing problems such as black soil degradation[2]. Obstacles to cultivated land production are particularly prominent, and the ecological quality of farmland needs to be restored[3].

The black soil layer is highly viscous and has a fragile mechanical structure. It is easily destroyed by mechanical compaction, resulting in the destruction of the aggregate structure and formation of a plow bottom layer[4]. The bearing characteristics of the tillage layer are related to the soil settlement index, cohesive modulus, friction modulus, and other parameters, which are related to soil cohesion, soil shear resistance angle, and shear deformation parameters[5], and its internal stress transfer is related to the stress concentration coefficient[6]. Therefore, when the soil moisture content is high and the compaction degree is low, the soil bearing and shear capacities are reduced. The black soil tillage layer is a viscous soil. When the unit is operating, it exerts a certain load and friction on the tillage layer soil, which is prone to unit sinking and drive-wheel slippage[7].

Land preparation is at the core of conservation tillage. It can loosen the soil, break up the plow bottom layer, increase the contact area between the soil and air, increase the amount of rainwater infiltration, increase the soil moisture content and porosity, ensure that the roots of crops can fully absorb oxygen and water, and simultaneously improve the quality of cultivated land, increase soil fertility, improve the soil's ability to retain moisture and resist drought, ensure air circulation in the deep plow layer, and make internal microorganisms more active[8]. Deep tillage has been widely promoted and applied in foreign agricultural production. At present, our country is vigorously promoting conservation tillage, and deep tillage technology has also been promoted. There is a large demand for deep tillage technology, machinery, and equipment in the country's agricultural production. The "National Agricultural Machinery Deep Tillage and Land Preparation Operation Implementation Plan (2016-2020)" pointed out that in 2016, the

Received date: 2025-04-27 **Accepted date:** 2025-06-12

Biographies: **Xiao Yang**, PhD, Associate Professor, research interest: agricultural machinery ground mechanics, Email: yangxiao2020@cau.edu.cn; **Hongrui Hu**, Undergraduate, research interest: agricultural machinery ground mechanics, Email: 3119585935@qq.com; **Xianglei Liu**, MS, research interest: agricultural machinery ground mechanics, Email: 3150341717@qq.com; **Junhao Huang**, MS, Associate Professor, research interest: vehicle system dynamics, Email: 396062782@qq.com.

***Corresponding author: Wenjie Li**, MS, Teaching Assistant, research interest: vehicle system dynamics. Logistics Academy, Xuzhou 221000, Jiangsu China. Tel: +86-15252184231, Email: liwenjiecau@163.com.

country planned to implement 10 005 000 hm^2 of agricultural machinery deep tillage and land preparation; in 2017, the country planned to implement 11 005 500 hm^2 of the same; and in 2018, 2019, and 2020, the country planned to implement 12 673 000 hm^2. At present, deep tillage and land preparation are included in the scope of new comprehensive subsidies for agricultural inputs[9].

It is necessary to determine the physical parameters of the soil when heavy tractors are used for land preparation. When the soil is compacted, the depth of the deep tillage should be reduced as much as possible. If the tillage depth is too large, it will cause excessive resistance to the unit and even damage the machine[10]. When the soil is compacted, deep tillage must be completed by combining it with shallow tillage. The first deep tillage depth was controlled at approximately 5-10 cm, and the depth was increased by 5 cm each time. Through multiple deep tillage operations, the plow bottom layer is gradually broken to avoid damage to parts owing to excessive resistance of the machine and to ensure the requirements of agronomic specifications. The combination of deep tillage and shallow tillage can provide the tillage layer with a more reasonable tillage layer structure[11].

Compaction of the plow layer by large tractors has a temporal and spatial accumulation effect, which seriously affects the efficiency of tillage and land preparation. Mechanized links such as tillage, management, harvesting, and transportation not only compact the physical, chemical, biological, and other ecological structures of the plow layer at different depths in space but also gradually show a compaction accumulation effect over time. Heavy agricultural machinery on farms in Northeast China has a serious soil compaction effect. When using it, there has been a lack of ecological protection for the plow layer soil. The long-term widespread use of mechanical shallow stubble removal and shallow rotary land preparation methods has not only caused a reasonable plow layer to become shallower, but also caused fine particles (silt particles and clay particles) in the soil state to be rotated into flour, the aggregate structure to be destroyed, and the plow layer to become shallower. Compared with the middle of the last century, the average thickness of the black soil layer has dropped from 50 to 60 cm to approximately 30 cm, and the organic matter content of the plow layer soil has decreased by approximately 50%-60%. The problem of degradation of the ecological structure of the physical, chemical, and biological plow layer has become very serious[12].

In terms of tire-terrain mechanics models, foreign scholars have established tire-soil empirical models, such as Wismer and Stiremod et al.[13-16] Bekker et al.[17] established a widely used tire-terrain mechanics model based on Bernstein's semi-empirical model[18]. The soil is regarded as an elastic-plastic body. According to the difference between the soil and tire types, the deformation contact characteristics of the tire and soil are considered, and the tire is regarded as an elastic body or a rigid body mechanics model.

In terms of the mechanism of agronomic stress caused by compaction of the tillage layer, domestic and foreign scholars mainly studied the interaction process between agricultural machinery and soil through tire-soil model, discrete element simulation, field test, and other methods. Wang et al.[19] investigated the stress transfer mechanism of soil under static or dynamic loads with straw mulching. The study indicated that the shock-absorbing effect of straw is strongest under low-stress static loads. Grünberg et al.[20] studied the impact of harvesting operations using harvesters and forage harvesters on soil properties. The results showed that after harvesting operations, the average rut depth was 13 cm. The maximum penetration resistance occurred at 10-15 cm, highlighting the significant impact of harvesters and loaders at this depth. Yang et al.[21] investigated the interaction mechanism between the driver, agricultural machinery, and black soil. The results indicated that seeding operations have a significant impact on soil compaction, and the findings can provide references for integrating human-factor efficiency with conservation tillage. For example, Keller et al.[22] used the SoilFlex model to input agricultural machinery and soil parameters, and output the soil stress-strain relationship to reflect soil compaction; Castioni et al.[23] used the SoilFlex model to simulate the tire contact area and the stress transmitted to the soil during straw removal, and then evaluated the degree of change in soil physical indicators; Bilson et al.[24] reported that soil hydraulic properties may be a more sensitive indicator of the impact of soil compaction on soil structure and pore system function; and Temitope et al.[25] collected undisturbed soil samples in two sampling directions, four depths, and three different locations, and proved that with the increase of medium and coarse pore components in the soil, the pore water pressure may remain unchanged or decrease.

In terms of the tillage layer stress transfer model, He et al.[26,27] analyzed the soil stress transfer coefficient based on the soil compaction model, and used soil stress sensors to conduct field tests to study the soil stress transfer coefficient at different depths under different loads. The results showed that with an increase in soil depth, the soil stress transfer coefficient decreased significantly, indicating that the soil stress gradually decayed during transfer to the deep soil layer. Wang et al.[28] studied the stress transfer of the tillage layer soil in no-tillage farming based on the nonlinear elastic-plastic contact model extended by discrete element software. The soil stress transfer of the tillage layer was studied by calibrating and optimizing the parameters, and the simulation model and measured soil stress transfer characteristic curves were compared and analyzed. Thus, the model was verified to be highly accurate. Zhong et al.[29] analyzed the soil stress transfer characteristics of the tillage layer in the corn stalk-soil mixed state based on the discrete element contact model.

In the past, the ground mechanics model was only constructed for the tire and ground, which resulted in the failure to link the plow layer stress model with the unit. As a result, the degree of compaction of the plow layer by tires was uncontrollable during actual mechanized operations. Therefore, it is necessary to consider the operating dynamics model of the tractor unit and integrate it to construct a plow-layer stress model. This study focuses on new requirements for the ecological operations of agricultural machinery in the new era. Aiming at the unclear effect of the mechanical stress of heavy tractors combined with land preparation units on the compaction of the plow layer soil, a "heavy tractor-plow layer soil" system dynamic coupling model was constructed from the perspective of agronomy and agricultural machinery integration. The main influencing factors of combined land preparation operations on the compaction of the plow layer were analyzed, the response law of the plow layer compaction process to the plowing unit parameters was explored, and experimental verification was carried out.

2 Materials and methods

2.1 Kinematic model of heavy-duty tractor unit

The soil conditions in Northeast China are good, and the terrain is relatively flat. Therefore, the lateral movement of the tractor is ignored in this study, and it is assumed that the heavy tractor unit travels in a straight line during land preparation operations[30,31]. The

straight line perpendicular to the ground where the tractor's center of mass T_0 is located is taken as the Z-axis, and the straight line parallel to the ground is taken as the X-axis. A rectangular coordinate system XOZ was established, and the origin of the coordinate system was the intersection point O of the X- and Z-axes. When the tractor is stationary, the soil exhibits no subsidence, the front and rear wheels are not deformed, and the front and rear wheels are on the same horizontal plane. The geometric relationship between the front and rear axles and the center of mass of the tractor is shown in Figure 1.

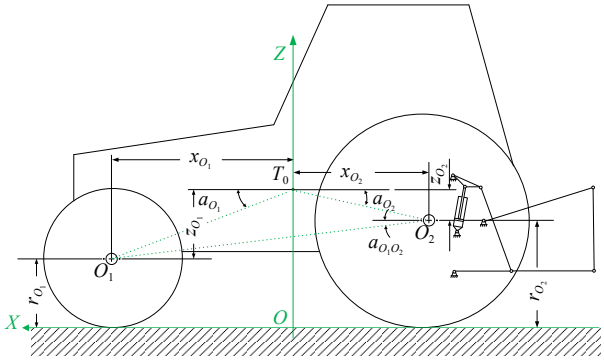

Figure 1 Geometric relationship of tractor front and rear axle and centroid position

$$\begin{cases} \alpha_{O1} = \arcsin\left(\dfrac{r_{O2}-r_{O1}}{l_{O1O2}}\right) \\ x_{O1} = l_{O1O2}\cos\alpha_{O1O2} - x_{O2T0} \\ z_{T0} = r_{O2} + z_{O2T0} \\ z_{O1T0} = z_{T0} - r_{O1} \\ l_{O1T} = \sqrt{z_{O1T0}^2 + x_{O1T0}^2} \\ l_{O2T} = \sqrt{z_{O2T0}^2 + x_{O2T0}^2} \\ \alpha_{O1T0} = \arctan\dfrac{z_{O1T0}}{x_{O1T0}} \\ \alpha_{O2T0} = \arctan\dfrac{z_{O2T0}}{x_{O2T0}} \end{cases} \quad (1)$$

where, α_{O1O2} is the angle between the front and rear axle connecting line and the negative direction of the horizontal coordinate when the front and rear wheels of the tractor are not deformed, rad; l_{O1O2} is the distance between the front and rear wheel axles of the tractor, m; l_{O1}, l_{O2} are distance from the front and rear wheel axles to the center of mass of the tractor, m; z_{T0} is ordinate coordinate of the center of mass of the tractor's front and rear wheels when there is no deformation, m; r_{O1}, r_{O2} are geometric radius of the front and rear wheels of the tractor tire when there is no deformation, m; x_{O1}, x_{O2} are horizontal distance from the center of mass to the front and rear axles when the front and rear wheels of the tractor are not deformed, m; z_{O1}, z_{O2} are vertical distance from the center of mass to the front and rear axles when the front and rear wheels of the tractor are not deformed, m; α_{O1}, α_{O2} are angle between the center of mass of the tractor and the line connecting the front and rear axle centers when there is no deformation of the front and rear wheels, rad.

During the deep-tillage operation, the tractor and implement were connected through a suspension device. There are four hinge points A, B, M, and N on the tractor, as shown in Figure 2. A is the hinge point of the hydraulic cylinder; M is the upper hinge point. B is the lower hinge point, and N is the axis of the lifting arm. In order to determine the positional relationship between these four hinge points and the center of mass, the initial position coordinates are $A(x_{A0}, z_{A0})$, $B(x_{B0}, z_{B0})$, $M(x_{M0}, z_{M0})$, and $N(x_{N0}, z_{N0})$.

The hydraulic cylinder hinge points A, B, M, and N can be calculated according to the initial position coordinates. The distance calculation equation from each hinge point to the center of mass is as follows:

$$\begin{cases} l_{AT} = \sqrt{(x_{O2T0}-x_{A0})^2 + (z_{A0}-z_{O2T0})^2} \\ l_{NT} = \sqrt{(x_{O2T0}-x_{N0})^2 + (z_{N0}-z_{O2T0})^2} \\ l_{BT} = \sqrt{(x_{O2T0}-x_{Bv})^2 + (z_{B0}-z_{O2T0})^2} \\ l_{MT} = \sqrt{(x_{O2T0}-x_{M0})^2 + (z_{M0}-z_{O2T0})^2} \end{cases} \quad (2)$$

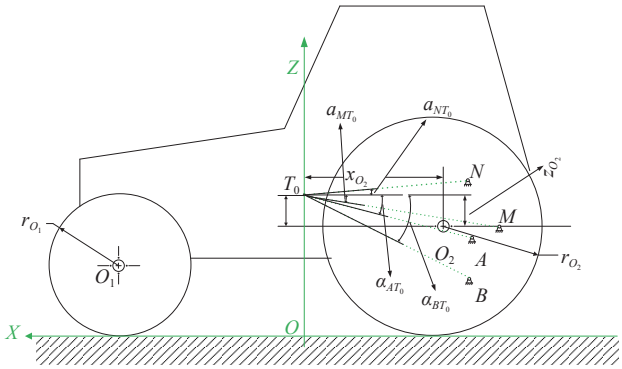

Figure 2 Each hinge point and axis position of tractor suspension device

When the tractor is stationary, the front and rear wheels are not deformed, and the ground contact points are on the same horizontal plane, hydraulic cylinder hinge point $A(x_{A0}, z_{A0})$, lower hinge point $B(x_{B0}, z_{B0})$, upper hinge point $M(x_{M0}, z_{M0})$, and lifting arm axis $N(x_{N0}, z_{N0})$ relative to the center of mass is calculated as follows:

$$\begin{cases} a_{AT0} = \arctan\left(\dfrac{z_{A0}-z_{O2T0}}{x_{O2T0}-x_{A0}}\right) \\ a_{NT0} = \arctan\left(\dfrac{z_{N0}-z_{O2T0}}{x_{O2T0}-x_{N0}}\right) \\ a_{BT0} = \arctan\left(\dfrac{z_{B0}-z_{O2T0}}{x_{O2T0}-x_{B0}}\right) \\ a_{MT0} = \arctan\left(\dfrac{z_{M_0}-z_{O2T0}}{x_{O2T0}-x_{M0}}\right) \end{cases} \quad (3)$$

2.2 Speed and acceleration of heavy-power tractors in transverse and longitudinal directions

Affected by the field topography, front and rear tire specifications, and front and rear axle load distributions, heavy tractors will have a certain pitch movement during field operations; that is, when the tractor is running, the position of the center of mass will not only change in X-direction but also in Z-direction (as shown in Figure 3). The tractor generates a certain angle α around the center of the mass. Angle α has a certain effect on the load distribution of the front and rear axles, as well as the size of the approach angle and departure angle of the front and rear tires, and then affects the ground area of the front and rear tires. In addition, when the machine is suspended, the pitch motion of the tractor changes the tractive force of the tractor on the machine, which significantly affects the working quality of the machine. Therefore, the running speed, acceleration, and rotation angle around the center of mass of the tractor in the X- and Z-directions have a significant impact on the soil pressure effect.

In order to facilitate the study of the motion state of the tractor, a stationary state is taken as the reference frame. This reference frame is a static reference frame, which can be used to calculate the position and center of gravity angle of the tractor during operation. The solution is as follows:

$$\begin{cases} x_T = x_{Ts} + x_T \\ z_T = z_{T0} + z_{Ts} + z_T \\ a_T = a_{Ts} + a_T \end{cases} \quad (4)$$

$$\begin{cases} \ddot{x}_T = a_{Tx}\cos a_T - a_{Tz}\sin a_T - \dot{z}_T\dot{a}_T \\ \ddot{z}_T = a_{Tx}\sin a_T + a_{Tz}\cos a_T + \dot{x}_T\dot{a}_T \end{cases}$$

where, x_{Ts}, x_T are the increment of the abscissa of the center of mass in the initial state and its change, m; z_{Ts}, z_T are increment of the longitudinal coordinate of the center of mass and its change in the initial state, m; α_{Ts}, α_T are angle of rotation of the tractor around the center of mass in the initial state and the increment of its change, rad.

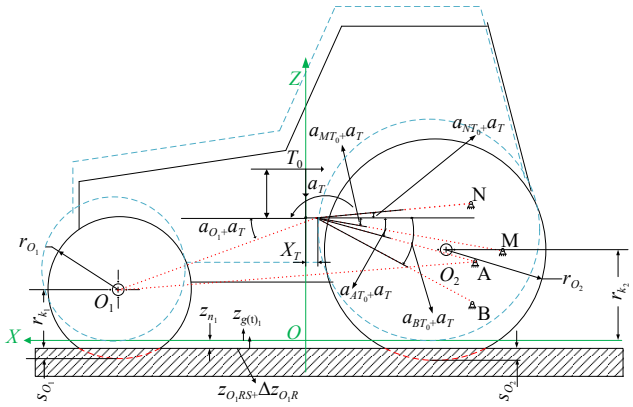

Figure 3 Tractor motion diagram

2.3 Dynamic model of heavy tractor unit

To fully consider the influence of various factors on the soil stress, it is necessary to establish a dynamic model for the entire heavy-duty subsoiling unit. In addition to the tractor in the horizontal and vertical directions, the force of the unit also includes the force on the agricultural machinery. The land pulley and subsoiling shovel are mainly dragged in the land preparation, in which the ground wheel is subjected to the horizontal support and rolling resistance of the soil, and the subsoiling shovel is subjected to the horizontal and vertical resistances of the soil and the gravity of the machine itself. The latter mainly includes the vertical support reaction of the front and rear wheels and the rolling resistance of the front and rear wheels. During the operation of deep loosening, the force received by the machine is transferred to the heavy tractor through suspension and hydraulic systems.

According to the force analysis in Figure 4, the equilibrium equation of the inertial force obtained from the horizontal resistance, tractive force, and center of mass based on horizontal acceleration can be listed, and the equilibrium equation of inertial force obtained from vertical gravity, support reaction, center of mass based on longitudinal acceleration, and moment balance equation of the tractor center of mass can be listed.

$$\begin{cases} Z_{K1} + Z_{K2} + F_{Rz} - F_{Vz} - F_G\sin a_G = m_T(g + a_{Tz}) + m_W(g + a_{Wz}) \\ F_{K1} + F_{K2} - F_{Vx} - F_G\cos a_G + -X_{K1} - X_{K2} - F_{Rx} - R_H = m_T a_{Tx} + m_W a_{Wx} \\ F_x(z_T - z_p - z_{rv}) - F_y(x_T - x_P) + F_{Rx}(z_T - z_U) + F_{Rx}(x_T - x_U) - \\ \quad F_{K1}[z_T - (z_{O1Rs} + Dz_{O1R})] - F_{k2}[z_T - (z_{O2Rs} + Dz_{O2R})] + \\ \quad X_{K1}(z_T - Z_{O1}) + X_{K2}(z_T - Z_{O2}) - Z_{K1}(x_{O1} - x_T) + Z_{K2}(x_T - x_{O2}) - \\ \quad m_w(g + a_{wz})(x_T - x_w) + m_w a_{wx}(z_T - Z_w) = J_T\ddot{a}_T - J_W\ddot{a}_V \end{cases} \quad (5)$$

Solving the above equations yields the longitudinal acceleration, vertical acceleration, and angular acceleration.

$$\begin{cases} a_{Tz} = \dfrac{Z_{K1} + Z_{K2} + F_{Rz} - F_y - F_{Vz} - F_G\sin a_G - m_W(g + a_{Wz}) - m_T g}{m_T} \\ a_{Tx} = \dfrac{F_{K1} + F_{K2} - X_{K1} - X_{K2} - F_{Rx} - F_x - F_{Vx} - F_G\cos a_G - m_W a_{Wx}}{m_T} \\ \ddot{a}_T = \dfrac{1}{J_T}[R_H(z_T - z_p - z_{rv}) - R_v(x_T - x_P) + F_{Rx}(z_T - z_U) + F_{Rx}(x_T - x_U) - \\ \quad F_{K1}[z_T - (z_{O1Rs} + Dz_{O1R})] - F_{k2}[z_T - (z_{O2Rs} + Dz_{O2R})] + \\ \quad X_{K1}(z_T - Z_{O1}) + X_{K2}(z_T - Z_{O2}) - Z_{K1}(x_{O1} - x_T) + Z_{K2}(x_T - x_{O2}) - \\ \quad m_w(g + a_{wz})(x_T - x_w) + m_w a_{wx}(z_T - Z_w) + J_W\ddot{a}_v] \end{cases} \quad (6)$$

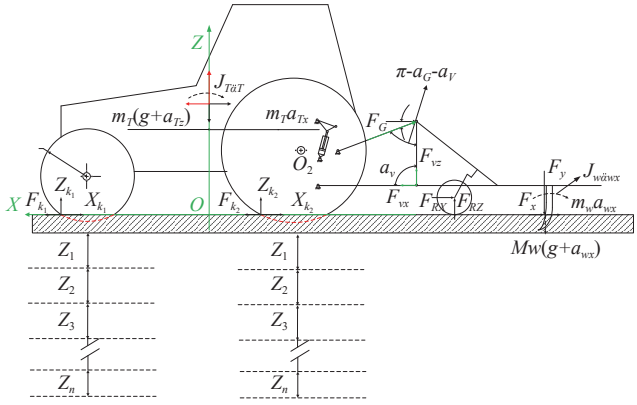

Figure 4 Tractor unit force diagram

2.4 Dynamic model of stress transfer in topsoil

2.4.1 Tire-soil contact force analysis

When a heavy-duty tractor performs field operations, the tire contacts the soil of the plow layer, and the load of the unit is transferred to the interior of the plow layer through the tire. The tractor tire is primarily subjected to a vertical load W, horizontal resistance F_T, and torque T exerted by the tractor and machinery. The surface soil exerts a combined reaction force F on the tire. The angle between the combined reaction force and vertical direction is α, and the distance between the combined reaction force and tire axis is e. The component of the combined reaction F in the horizontal direction is balanced with horizontal resistance F_T. The component of the combined reaction F in the vertical direction was balanced with vertical load W, and the torque T of the combined reaction F on the tire axis was balanced (Figure 5).

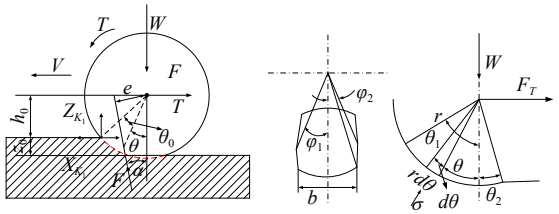

Note: θ is the angle along the contact surface; φ is the angle across the contact surface; Z_0 is the tire sinking, mm; b is the tire width, mm; h_0 is the distance between the wheel axle and the undisturbed soil surface, mm.

Figure 5 Tire-soil contact surface force diagram

When the tractor was stationary or moving at a constant speed, the equilibrium conditions were as follows:

$$\begin{cases} T - Fe = 0 \\ F\sin\alpha - F_T = 0 \\ F\cos\alpha - W = 0 \end{cases} \quad (7)$$

When the tractor moves uniformly in the horizontal direction, the rear wheel of the tractor is taken as the research object, the rear

wheel is the reference frame, and the coordinate system is established on the rear wheel. According to Newton's law of motion, the following can be obtained:

$$T/r - F\sin\alpha + F_{Ix} = 0 \tag{8}$$

where, T is torque applied by the rear drive shaft to the tire; r is radius of the rear wheel; T/r is driving force on rear wheels when the tractor is moving; F_{Iz} is inertial force on tractor; $F\sin\alpha$: horizontal component of the total reaction force of the ground on the tire, F_T.

The tire load calculation equation can be used to calculate wheeled non-road vehicles to decompose the tire surface into n small units. The soil stress on the tire contact surface is distributed on these n small units ΔS. The contact stress on each small unit can be decomposed into normal stress α and tangential stress τ. The torque T can be obtained by the double integration of the binary function shear stress $\tau(\theta,\varphi)$ in the transverse and longitudinal planes of the tire. The horizontal force T can be obtained by double integration of the horizontal components of shear stress $\tau(\theta,\varphi)$ and normal stress $\tau(\theta,\varphi)$ in the transverse and longitudinal planes. The calculation equation is as follows:

$$\begin{aligned} T &= \int_{\theta_2}^{\theta_1}\int_{\phi_2}^{\phi_1} r^3\tau(\theta,\phi)\,\mathrm{d}\theta\mathrm{d}\phi \\ F_T &= \int_{\theta_2}^{\theta_1}\int_{\phi_2}^{\phi_1}\left[\tau(\theta,\phi)\cos\theta - \sigma(\theta,\phi)\sin\theta\right] r^2\mathrm{d}\theta\mathrm{d}\varphi \\ W &= \int_{\theta_2}^{\theta_1}\int_{\phi_2}^{\phi_1}\left[\tau(\theta,\phi)\sin\theta + \sigma(\theta,\phi)\cos\theta\right] r^2\mathrm{d}\theta\mathrm{d}\varphi \end{aligned} \tag{9}$$

where, θ_1 is the approach angle and θ_2 is the departure angle. A schematic diagram of the approach and departure angles is shown in the figure below. The departure angle is calculated as follows. The departure angle is mainly determined by the tire pressure, tire wall stiffness, and soil cone index. Because the vertical component of the soil force on the tire and the tire vertical load W are a pair of balanced forces, they can be calculated based on this condition.

$$\theta_2 = \frac{\theta_m}{2}\left[1 - \left(\frac{p_i + p_c}{0.7CI - 0.6}\right)\right]^{\lambda} \tag{10}$$

where, θ_m is the center angle of the tire's contact length on a hard road, (°); p_i is tire pressure, kPa; p_c is tire sidewall stiffness, N/mm; λ is test constant; CI is soil cone index, kPa.

In the process of the stable operation of agricultural machinery, the resultant reaction force F plays a vital role in improving the power of agricultural machinery and has a direct impact on the compaction of surface soil. According to the above equation, the size of the resultant reaction force F is determined by the intersection position of F and the tire circumference, angle α, tire section width b, tire radius r, and stress distribution of the tire-soil contact surface.

The tire-soil contact surface boundary is modeled using the "super ellipse", and the boundary shape equation of the contact surface is:

$$\begin{aligned} &\frac{x^n}{a^n} + \frac{y^n}{b^n} = 1 \\ &\Omega = \left\{(x,y)\,\middle|\,\frac{x^n}{a^n} + \frac{y^n}{b^n} \le 1\right\} \end{aligned} \tag{11}$$

where, a is short half-axis of contact surface; b is long half-axis of contact surface; n is super-elliptic coefficient.

The contact area within a quadrant is:

$$A_{quadrant} = b\int_0^a \left(1 - \frac{x^n}{a^n}\right)^{\frac{1}{n}}\mathrm{d}x \tag{12}$$

Total contact area:

$$A = 4A_{\text{quadrant}} = 4b\int_0^a \left(1 - \frac{x^n}{a^n}\right)^{\frac{1}{n}}\mathrm{d}x \tag{13}$$

2.4.2 Dynamic model of soil stress transfer in the cultivated layer

Research on soil profile stress calculation is mainly based on the Boussinesq and Fröhlich equations to calculate the vertical stress state of the soil profile. The tire-soil contact area A(m²) was divided into i independent parts with an area of A_i (Figure 6). The vertical stress in each part is σ_i(kPa), $P_i = \sigma_i A_i$(kN). Under the condition of a vertical load P_i in this area, the vertical stress at any point on the soil profile with a depth of z is calculated as follows:

$$\begin{aligned} \sigma_z &= \sum_{i=0}^{i=n}(\sigma_z)_i = \sum_{i=0}^{i=n}\frac{vP_i}{2\pi}\frac{z_i^v}{r_i^{v+2}} \\ &\text{or} \\ \sigma_z &= \sum_{i=0}^{i=n}(\sigma_z)_i = \sum_{i=0}^{i=n}\frac{vP_i}{2\pi}\frac{z_i^v}{r_i^{v+2}}\cos^v\theta_i \end{aligned} \tag{14}$$

where, θ is the angle between the straight line from point load P_i to point and vertical plane; v is concentration coefficient during soil stress transfer; r is distance from the point of action of point load P_i to this point, cm.

When the loading force is evenly distributed on a circular contact surface with an equivalent radius of R, the vertical stress at z directly below the contact surface can be expressed as follows:

$$\sigma_z = \sigma_0\left[1 - \left(\frac{Z}{\sqrt{R^2 + Z^2}}\right)^V\right] \tag{15}$$

where, σ_0 is tire-soil contact stress, kPa; W is total load on the tire-soil contact surface, kg; σ_z is vertical stress at position z below the tire-soil contact surface, kPa.

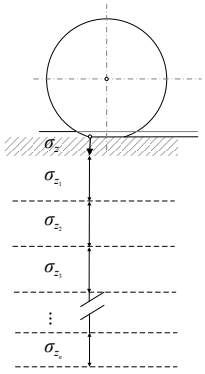

Figure 6 Internal stress transfer diagram of soil

2.5 "Heavy tractor-tilled soil" dynamic model coupling method

When a heavy tractor is working in the field, the implement and ground wheel are subjected to resistance from the soil. Each resistance can be decomposed orthogonally into X_{K2}, Z_{K2}, F_{Rz1}, F_{Rx2}, F_{y1}, F_{x1}, F_{Rz}, F_{Rx}, F_y, and F_x; the implement transmits resistance F_G, F_{Vx}, F_{Vz} to the tractor through the drawbar; the tractor applies vertical load W and torque T to the tire; and the tractor applies a total reaction force F to the road through its tires. F can be orthogonally decomposed into Z_{K1}, X_{K1}; the road load will be transferred to the tillage layer soil in the form of stress σ_z. As the soil depth increases, σ_z continues to decay, but it still causes compaction of the deep plowing layer.

Since the tractor and implement can be considered as a single unit during field operations, it is assumed that their motion states

are consistent, i.e., the lateral acceleration, longitudinal acceleration, and angular acceleration of the tractor and implements. Under the assumption of no slippage, the tractor's travel speed T is equal to the tangential speed at the tire edge; the resultant force of the road on the tire and the tire's force on the road form a pair of interacting forces; and the stress in the plow layer soil can be determined from the tire's pressure on the road. The various models are coupled using the aforementioned parameters. The tractor-implement model is coupled with the tire-soil model using the parameters in Equations (4) and (5), and the tire-soil model is coupled with the tillage layer stress model using the parameters in Equations (6) and (11).

Since the tractor and implement can be regarded as a whole during field operation, the motion state of the two is considered to be the same, that is, the lateral acceleration $\ddot{x}_T$, longitudinal acceleration $\ddot{z}_T$, and angular acceleration $\ddot{\alpha}_T$ of the tractor and the implement. Without considering slip, the tractor's travel speed is assumed to be equal to the linear speed ω_r of the tire edge. The resultant force F' of the road on the tire and F of the tire on the road are a pair of interacting forces; the stress σ_z of the tillage layer soil can be obtained by the pressure F of the tire on the road surface. The various models are coupled through the above parameters. The unit model is coupled with the tire-soil model through the relationship equation of the front and rear tire axis coordinate position and speed and the parameter $\ddot{x}_T = F_{Iz}/m$ in the torque balance equation. The tire-soil model is coupled with the tillage layer stress model through $F\cos\alpha/s = p_i$ in the kinematic analysis equation of the suspension mechanism. The coupling and load transfer processes are illustrated in Figure 7.

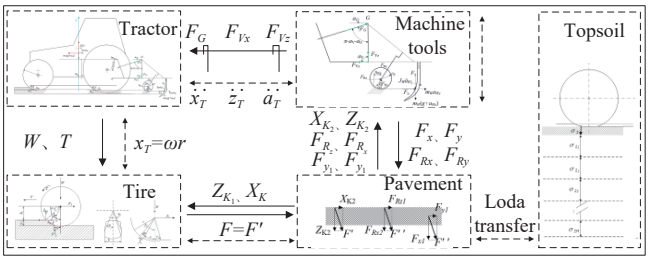

Figure 7 Coupling process and transfer mechanism of machine-agricultural machinery-pavement-tillage load model

3 Discussion

3.1 Heavy tractor-tillage soil model simulation verification

The unit-road surface-plow layer dynamic model is constructed, and Equation (16) is the longitudinal traction dynamic model of the heavy tractor unit. Within this equation, F_p is the traction force of the tractor, and f_x is the resistance of the tractor and the implement. The implement drag was calculated by multiplying the total mass of the tractor unit by the adhesion coefficient, where a is the acceleration of the unit.

$$F_p - f_x - f_j = ma \tag{16}$$

Equation (17) is the dynamic model of the longitudinal traction force of the tire, where T is the drive shaft torque, r is the tire radius, F is the total reaction force of the road on the tire, $F\sin\alpha$ is the longitudinal component of the total reaction force of the road on the tire, and m_1 is the tire mass:

$$T/r - F\sin\alpha = m_1 a \tag{17}$$

Equation (18) is for calculation of non-road vehicle tires. The contact stress on each tiny unit of the tire-soil contact surface can be decomposed into normal stress σ and tangential stress τ, where θ_1 is the approach angle, θ_2 is the departure angle, r is the tire radius, b is the tire width, and $F\sin\alpha$ is obtained by integrating the horizontal components of shear stress $\tau(\theta,\varphi)$ and normal stress $\sigma(\theta,\varphi)$ in the transverse and longitudinal planes.

$$F\sin\alpha = rb\int_{\theta_2}^{\theta_1}[\tau(\theta)\cos\theta - \sigma(\theta)\sin\theta]\,\mathrm{d}\theta \tag{18}$$

$$\theta_2 = \frac{\theta_m}{2}\left[1-\left(\frac{p_i+p_c}{0.7CI-0.6}\right)\right]^{\lambda} \tag{19}$$

$$p = \frac{F_T\cos\alpha}{(\theta_1+\theta_2)rb} \tag{20}$$

Equation (21) is for calculation of the vertical stress of soil profile. P is the vertical load on the tire-soil contact surface, v is the stress concentration coefficient during soil stress transfer, r is the distance from the point of action of surface soil stress P to this point, and z is the calculated plowing layer depth.

$$\begin{aligned}\sigma_z &= \frac{vPz^v}{2\pi r^{v+2}}\\ \sigma_z &= \sum_{i=0}^{i=n}(\sigma_z)_i = \sum_{i=0}^{i=n}\frac{vP_i}{2\pi}\frac{z_i^v}{r_i^{v+2}}\cos^v\theta_i\end{aligned} \tag{21}$$

A mechanical model of the unit-pavement-plow layer system was built in Simulink, and the measured traction, soil compaction, and soil depth corresponding to different times in the field test were used as inputs (Figure 8 and Table 1). Finally, the model output the soil stress value of the plow layer at the corresponding depth. The soil stress value output by the model was compared with the stress value measured in the field to verify the accuracy of the model.

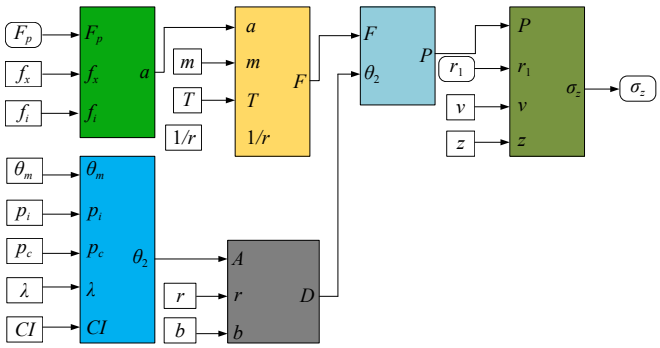

Figure 8 Mechanical model of unit-pavement-tillage system

Table 1 Parameter setting of simulation model

	Parameters	Values
Land preparation unit	Tractor quality (m_1)	7770 kg
	Machine quality (m_2)	1000 kg
	Rated engine speed (n)	2100 r/min
	Rated power (hp)	205 horsepower
	Adhesion coefficient (μ)	0.5
Front tire (420/90R30)	Tire outer diameter (r)	762 mm
	Tire width (b)	420 mm
Rear tire (480/80R46)	Tire outer diameter (r)	1168.4 mm
	Tire width (b)	480 mm
Soil type	Soil cohesive modulus (k_c)	24.9×10^3 N/m^{n+1}
	Soil friction modulus (k_φ)	3.573×10^6 N/m^{n+2}
	Subsidence index (n)	1.09
	Soil cohesion (c)	2.5×10^3 N/m^2
	Shear resistance angle (φ)	28.2°
	Shear deformation parameters (K)	0.041 m
	Stress concentration factor (v)	2

The measured traction force and distance and the corresponding tillage layer depth in the field test were input, and various parameters in the model were set. The tillage layer soil stress data output by the unit pavement-tillage layer system mechanical model built in Simulink was compared with field-measured soil stress data. The simulation and measured data are shown in Figure 9. Therefore, through the simulation of the mechanical model of the unit-pavement-plow layer system and the comparative analysis of the field-measured data, the established mathematical model can more accurately reflect the stress characteristics of the plow layer soil caused by the heavy tractor land preparation operation.

The pressure on the surface soil can be calculated by Equation (20). It is calculated by dividing the vertical component of the tire-soil force by the area of the contact surface $(\theta_1+\theta_2)rb$.

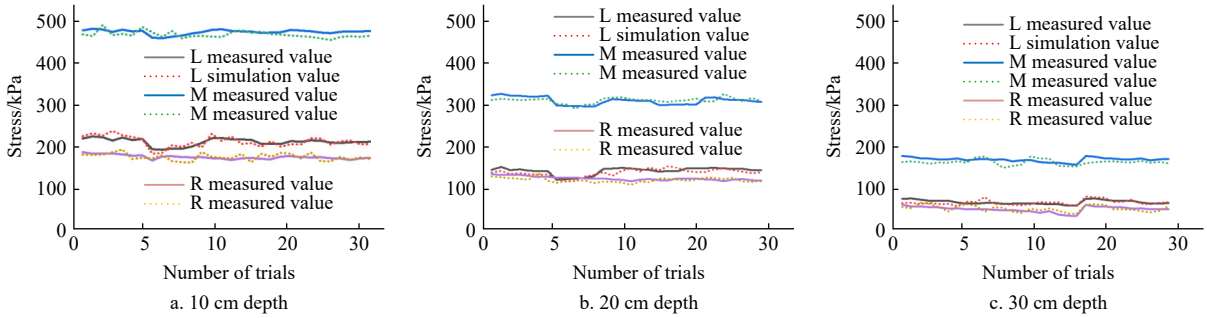

Figure 9 Soil stress of plow layer at different depths

4 Results verification

4.1 Overview of the test area

The test area was located in Block 1-3, Zone 3, Jianshan Farm, No. 93 Bureau of Beidahuang farmland recreation (125°30′E, 48°54′N). The soil type was sandy loam. The deep tillage unit used a 220-horsepower heavy-duty tractor (rear wheel 480/80R46, air pressure 1.8 bar). The supporting equipment used was a combined land preparation machine with deep tooth loosening. The operating speed was adjusted according to the test content. The total weight of the land preparation unit was approximately 10t when fully loaded.

4.2 Experimental plan

The tractor parameters mainly include real-time tire pressure, vehicle speed, tire speed, slip rate, acceleration, and tire contact area. RACELOGIC BOX sensor is used to test real-time tire pressure, vehicle speed, tire speed, slip rate, acceleration and other data; vibrating wire soil press is used to test soil internal stress; GPS antenna, acceleration sensor, etc. are integrated in RACELOGIC BOX. Tire pressure sensor is installed on the valve stem, and nine-axis attitude angle sensor is installed on the tire (Figure 10).

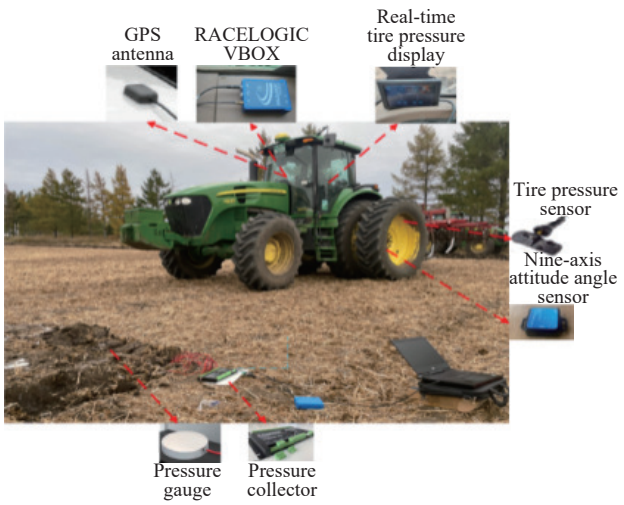

Figure 10 Field experiment system of tractor

4.2.1 Experimental verification of the influence of unit operating parameters on soil stress transfer

The VBOX RACELOGIC vehicle test system is based on a high-tech satellite receiver that integrates multiple modules. It is mainly used to measure the vehicle speed, acceleration, driving trajectory, heading angle, longitude and latitude, fuel consumption, tire pressure, slip rate, and other parameters. Its main features include powerful functions, the ability to test multiple parameters, and the ability to match the required sensors according to the test requirements. In this test, tire pressure sensors and nine-axis attitude angle sensors were installed based on the test content. The tire pressure sensor was connected to a display screen that could collect and display the tire pressure in real time. A nine-axis attitude angle sensor was used to test the angular velocity of the wheel. Combined with the vehicle speed collected by the VBOX, real-time slip rate data can be collected. As shown in Figure 11, the internal configuration structure and data-reading interface of the VBOX RACELOGIC vehicle test system are integrated with multiple modules and equipped with a memory card. The collected test data can be recorded on the memory card, and the test data can be read using the analysis software on the PC.

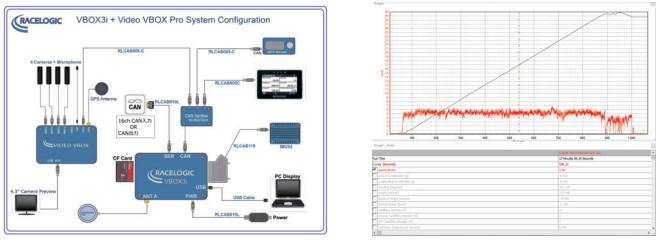

a. VBOX system structure b. Data reading interface

Figure 11 VBOX RACELOGIC test system

4.2.2 Soil stress test of cultivated layer

Owing to the large mass of heavy tractors and their vibration and impact during operation, they exert great stress on the surface and interior of the soil. This stress causes the soil compaction to increase sharply, and the water content to drop sharply. Repeated rolling causes the soil to become compact. To verify the influence of various parameters on soil compaction during unit operation, the soil stress data of the tillage layer were collected during the deep loosening operation of the unit, as shown in Figure 12.

A vibrating-wire earth pressure gauge is used to measure the internal stress of the soil. An earth pressure gauge is an embedded pressure sensor that can be connected to a PC or display test data

a. Buried location of soil pressure gauge in tillage layer

b. Soil stress and pressure acquisition equipment

Figure 12 Tillage stress acquisition equipment

through a data acquisition instrument or wireless communication. It is mainly used to measure the stress of the soil inside structures, such as earth-rock dams, earth embankments, slopes, roadbeds, retaining walls, and tunnels. The main components of the sensor were made of special steel and could be used in harsh environments. It exhibits excellent performance, good accuracy and sensitivity, excellent waterproofing performance, corrosion resistance, and long-term stability. After improving cable protection measures, it can be directly buried in compacted soil with high instrument requirements. First, the initial frequency of the vibrating wire earth pressure gauge is calibrated. The frequency increased when the pressure gauge was subjected to a load. The initial frequency and the frequency value at time i are converted into the stress value at this time through the conversion relationship shown in Equation (22). The compressive stress P of the vibrating wire earth pressure gauge can be calculated.

$$P = K(f_i^2 - f_0^2) + K_t(T_i - T_0) \tag{22}$$

where, P is measured compressive stress value, MPa; K is linear relationship coefficient between output frequency value and compressive stress, MPa/Hz^2; f_i is frequency at time i, Hz; f_0 is reference frequency in the initial state, Hz; K_t is relationship between compressive stress and temperature; T_i is temperature during measurement, °C; T_0 is temperature during factory inspection and calibration, °C.

The signal collected by the pressure gauge was a vibrating string signal, and the corresponding collector was required to read the vibrating string signal. The VTN-416 vibrating string signal collector selected for this test was a multichannel vibrating string, temperature, and analog sensor signal collector (Figure 13). It can simultaneously collect vibrating strings and analog signals at the same time. It has a 48-channel sensor interface and a 16-channel DAC output. It can perform real-time or fully automatic timing collection and storage of up to 32-channel vibrating string frequencies, 32-channel temperature sensors (thermistors or DS18B20), and 32-channel analog sensors (voltage or current) (support external U-disk). One adjustable power supply output can power other sensors: a programmable multichannel 16-channel DAC output, which can be used to convert the frequency signal of the vibrating string sensor into an analog signal or programmable control in real time, and the RS485 data interface, industrial MODBUS, or custom AABB simple communication protocol can be directly connected to the existing measurement and control system.

The VTN-416 vibrating string signal acquisition instrument has four working modes: power-on self-start, manual start, timed acquisition, and command drive. Considering that the test required a short acquisition time interval, the power-on self-start mode was selected for this test. In this mode, as long as the external power supply is connected, the acquisition instrument is always in a power-on state and never shuts down. The VTN automatically stores and sends data at time intervals preset by the parameters.

Figure 13 VTN-416 multichannel vibrating wire signal acquisition instrument

Before the tractor performs field operations, a pit approximately 50 cm deep is dug from the edge of the working path and a groove is dug from the side of the pit. During this process, a level is required to detect whether the surface of the groove is flat. If it is not flat, the data measured by the pressure gauge are inaccurate. After the surface was flat, the press was placed in the groove, and three pressure gauges were placed at depths of 10, 20, and 30 cm to measure the soil stress at different depths. Simultaneously, the stress distribution of the contact surface between the tire and soil can also be measured (Figure 14).

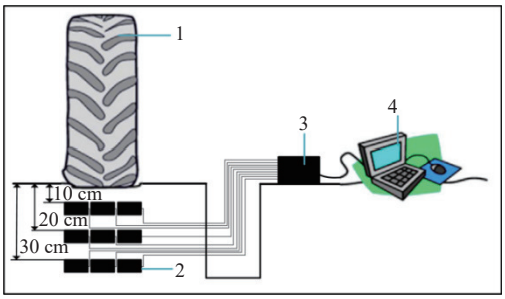

1. Tire 2.Vibrating wire earth pressure gauge 3.VTN-416 vibrating-wire collector 4. Laptop

Figure 14 Layout scheme of soil stress meter

When the unit passes over the pressure gauge, the analysis software of the host computer can detect changes in the frequency value over time. In this test, the pressure gauge collected data at a frequency of 40 ms/time.

4.3 Experimental verification of the influence of unit operating parameters on soil stress transfer

4.3.1 Heavy-duty land preparation unit operation data

The VBOX records the data in the memory card. The data files in the memory card were parsed using the VBOX Test Suite software. In total, 10 764 sets of data were obtained after parsing. A portion of the representative data was selected. The maximum driving speed was 5.558 km/h, and the minimum was 3.6 km/h. The speed fluctuated within this range during operation, with an average

speed of 4.67 km/h. The slip rate fluctuated between 0%-58%. The slip rate is generally positively correlated with vehicle speed. When the vehicle speed is higher, that is, the driving-wheel speed is higher, the tractor wheels are prone to slip. Some data points may not show an obvious positive correlation owing to the influence of road conditions because the slip rate is also affected by the contact conditions between the tire and the road. The greater the speed, the smaller the acceleration. When the acceleration is zero and the acceleration directions on the left and right sides are different, the speed reaches an extreme value. The lateral acceleration fluctuates around 0, and the overall average value is approximately 0, because the lateral acceleration affects the heading angle. When the lateral acceleration is not zero for a long time, the driving direction of the tractor deviates from the established direction. Therefore, to maintain the correct running direction, the lateral acceleration fluctuates at approximately 0. Affected by the farmland terrain, the vertical acceleration is kept below 0, fluctuating between –0.3 to 0 m/s^2 (as shown in Figure 15).

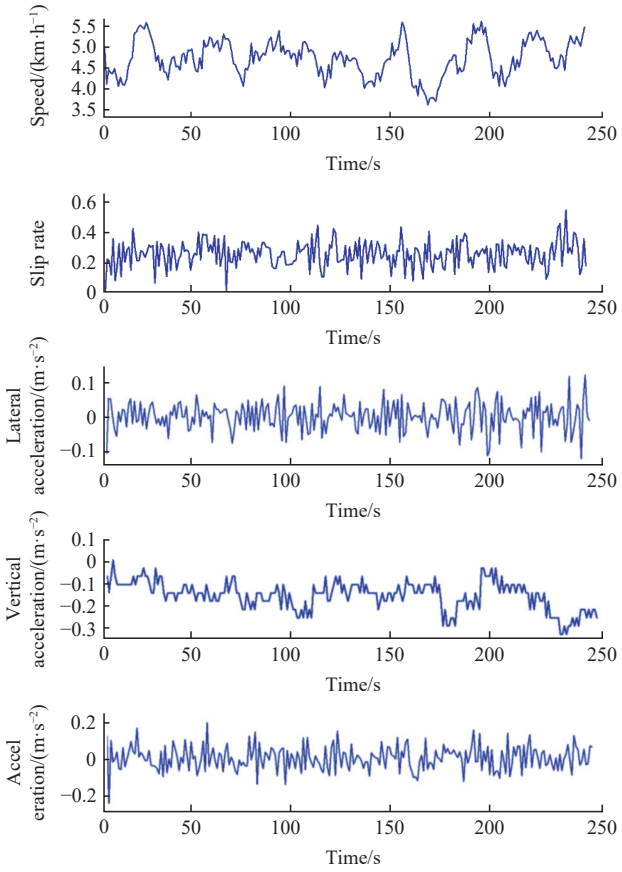

Figure 15 Field trial data

4.3.2 Effect of heavy unit operating speed on soil stress transfer

During the field operation of heavy tractors, pressure gauges were buried at multiple locations to measure the stress applied to the soil by the heavy units during land preparation operations. Because of the large tire width, three pressure gauges were buried at each tillage depth. After the pressure gauges were buried, the tractor was allowed to compact back and forth several times. The experimental data were measured after the soil compaction was relatively large to minimize the impact of soil compaction on the test data. During the experiment, the soil stress of the heavy land preparation unit was measured at 3 km/h, 6 km/h, and 9 km/h. The black curve represents the stress applied by the inner side of the tire to the tillage layer soil; the red curve represents the stress applied by the middle position of the tire to the tillage layer soil; and the blue curve represents the stress applied by the outer side of the tire to the tillage layer soil; the dotted line represents simulated data. The above tires are the left rear wheels of the tractor.

Figure 16 shows the soil stress data when the heavy-duty land preparation unit performs field land preparation operations at different speeds. From the test data, it can be observed that with an increase in the number of tests, the soil stress shows a gradual downward trend. The soil stress at a depth of 10 cm was significantly greater than that at depths of 20 cm and 30 cm. This is because the stress on the surface soil is the largest, according to the internal stress transfer model of the cultivated soil. With increasing depth, the soil stress decreased sharply. Combined with the soil-stress curves at different operating speeds, the soil stress continued to decrease as the operating speed increased. When the operating speed is 3 km/h, the soil stress at a depth of 10 cm can reach a maximum of 499.2 kPa; when the operating speed is 9 km/h, the soil stress at a depth of 10 cm is 469.1 kPa, which is 6% lower than the operating speed of 3 km/h; when the operating speed is 9 km/h, the soil stress at a depth of 10 cm is 438.8 kPa, which is 12% lower than the operating speed of 3 km/h. The soil stress at depths of 20 and 30 cm also decreased accordingly, but the soil stress at a depth of 10 cm was the most obvious.

4.3.3 Effect of heavy-duty unit operation acceleration on soil stress transfer

As the data collected by the pressure gauge and VBOX have corresponding times, the stress value applied to the tillage layer soil when the tractor operates at different accelerations can be measured. Figure 17 shows the relationship between the tractor acceleration and soil stress. With the increase in lateral acceleration and longitudinal acceleration, the soil stress shows an upward trend because lateral acceleration and longitudinal acceleration are provided by the lateral and longitudinal components of the soil's total reaction force on the tire. When the tractor drives and the wheel slips, the tractor tire is subjected to friction opposite to the relative movement direction of the contact surface. When the acceleration increased, the shear stress τ increased accordingly, resulting in shear stress τ and normal stress σ. When the longitudinal acceleration reached 0.2 m/s^2, the soil profit at 10 cm tended to be stable. At this time, the total reaction force F of the soil increases, and the stress applied by the tire to the soil also increases. Unlike longitudinal acceleration, when the direction of lateral acceleration changes, the soil stress inside the tire changes in an opposite manner to that of the external soil stress. When the tractor's lateral acceleration is directed toward the outside of the tire, the soil stress outside the tire increases, whereas the soil stress inside the tire decreases. When the tractor's lateral acceleration is directed toward the inside of the tire, the soil stress inside the tire increases, whereas the soil stress outside the tire decreases. This is because when the tractor has lateral acceleration, the center of mass position shifts in the direction of acceleration, causing the load distribution to change and affecting the soil stress distribution pattern.

4.3.4 "Heavy tractor-tillage soil" model testing and verification

Soil stress data was collected during field trials under different tractor operating speeds, longitudinal acceleration, and vertical acceleration conditions. To verify the accuracy of the model, the correlation coefficient between the experimental data and the simulated data was calculated. The results are listed in Tables 2-4. The results indicate that the correlation coefficient is approximately equal to 1, indicating high model accuracy, which can be used to accurately calculate soil stress under different operating conditions.

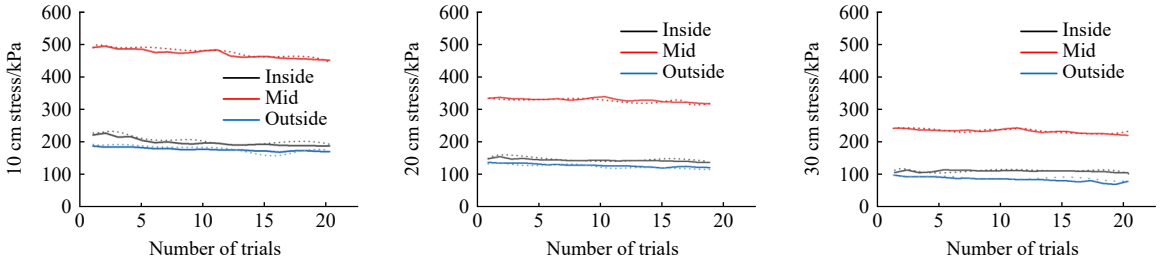

a. Soil stress at tractor speed of 3 km/h

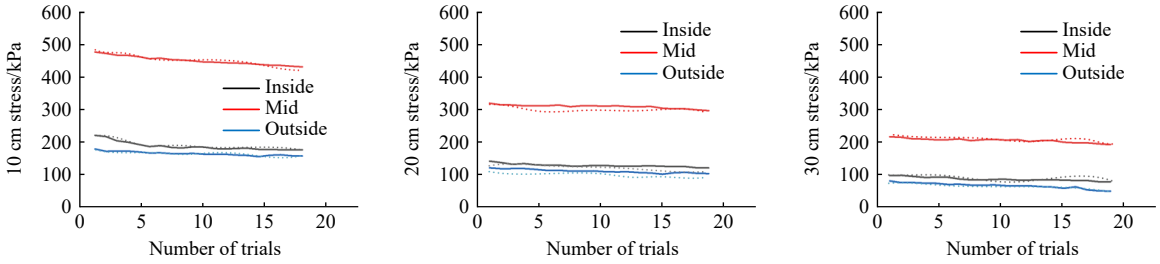

b. Soil stress at tractor speed of 6 km/h

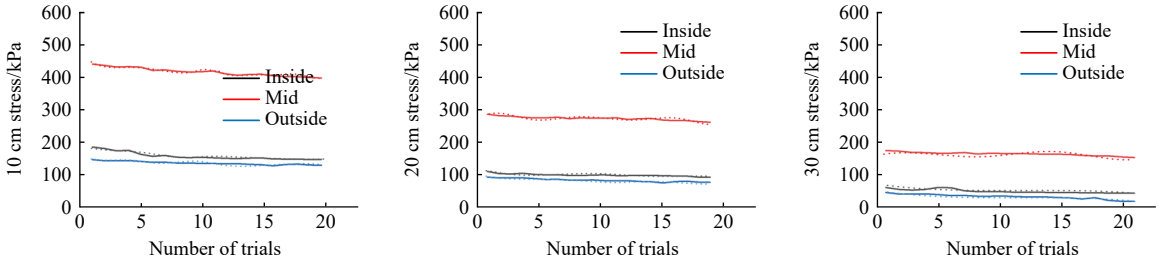

c. Soil stress at tractor speed of 9 km/h

Figure 16 Soil stress at different operation speeds

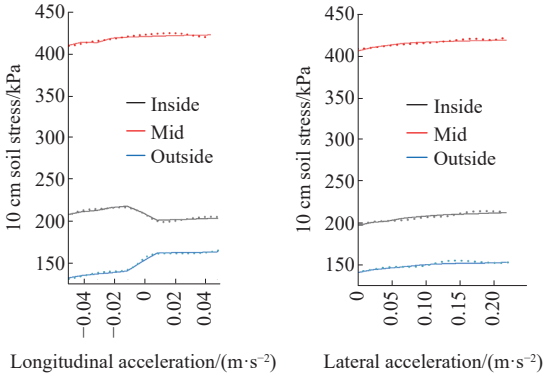

Figure 17 Tractor acceleration velocity-soil stress

Table 2 Correlation coefficient-*v*

Speed/km·h^{-1}	*r*
3 (Inside)	0.85
3 (Mid)	0.87
3 (Outside)	0.79
6 (Inside)	0.81
6 (Mid)	0.82
6 (Outside)	0.75
9 (Inside)	0.82
9 (Mid)	0.80
9 (Outside)	0.71

Table 3 Correlation coefficient-a_1

Longitudinal acceleration/m·s^{-2}	*r*
0-0.2 (Inside)	0.75
0-0.2 (Mid)	0.77
0-0.2 (Outside)	0.73

Table 4 Correlation coefficient-a_2

Lateral acceleration/m·s^{-2}	*r*
–0.04-0.04 (Inside)	0.76
–0.04-0.04 (Mid)	0.75
–0.04-0.04 (Outside)	0.71

5 Conclusions

This study investigated the soil compaction problem caused by heavy-duty units in field operations. Based on the mechanical model of the "tractor-machine-tire-soil-plow layer" system, a theoretical analysis was performed. The mechanical models of each subsystem were studied, and the models of each part were coupled to analyze the load transfer process and the influence of each parameter in the model on soil stress, which helps to alleviate soil compaction. The main conclusions are as follows:

(1) The stress transfer model of the tillage layer and its coupling mechanism were studied.

(2) As the number of compaction cycles increased, soil stress transfer showed a gradual decreasing trend.

(3) As the working speed increased, soil stress continued to decrease, with the most significant decrease observed at a depth of 10 cm.

(4) When the lateral and longitudinal acceleration of the unit increases, it affects the distribution of stress applied to the soil by the tires. The stress on the inner side of the tires changes in the opposite direction to that on the outer side.

Acknowledgements

This work was funded by the National Natural Science Foundation of China (Grant No. 32201671).

[References]

[1] Wang X L, Wang Q J, Li H W, Li W Y, Niu Q, Chen W Z. Effect of tyre induced soil compaction on soil properties and crop root growth under no-tillage system. Transactions of the CSAM, 2017; 48(6): 168–175.

[2] Li B G, Ren T S, Liu Z, Huang F, Yang X G, Liu Z J, et al. Consolidating the granary of black land to ensure national food security. Journal of the Chinese Academy of Sciences, 2021; 36(10): 1184–1193.

[3] Yin C J. Effectively increasing the protection and construction of arable land and firmly guarding the red line of 1.8 billion mu. China Reclamation, 2022; 4: 4–8.

[4] Li R. Black soil conservation and cultivated land quality improvement. Humic Acid, 2023; 1: 13–22.

[5] Gong H H. Finite element analysis and structure optimization for subsoiling shovel based on soil mechanics model. Xihua University, 2013. DOI: 10.7666/d.D345843 (in Chinese)

[6] Zhang S, Wu Z B, Chen J, Li Z, Zhu Z X, Song Z H, et al. Control method of driving wheel slip rate of high-power tractor for ploughing operation. Transactions of the CSAE, 2020; 36(15): 47–55.

[7] Li L, Huang B H, Zeng J H, Liu M H, Li J, Xue L. In-situ test analysis on mechanical properties of paddy surface soil. Journal of Hebei Agricultural University, 2023; 46(1): 121–126.

[8] Wang Q J, Jiao F, Han D L, Sui Y G, Yang X Y, Wang X D, et al. Impact of different mechanical soil preparation methods on physical and chemical properties of soil in low-lying paddy fields and rice yield. Transactions of the CSAE, 2019; 35(18): 70–77.

[9] Lin Z K. Optimization and experiment of combined subsoliler. Northwest Agriculture and Forestry University, 2016. (in Chinese)

[10] Gao Z C, Song B Q, Wang C L, Gao W C, Zhang L L, Sun L, et al. Soil amelioration by deep ploughing of different machineries and its effect on promoting crop growth and yield. Transactions of the CSAE, 2018; 34(12): 79–86.

[11] Gao Y P. Summary of the main forms and operating standards of mechanized deep pine land preparation. Agricultural Machinery Use and Maintenance, 2021; 1: 135–136.

[12] Kang D X. Design and research on subsoiling, stubbling and suppress soil crushing combined tillage machine. Gansu Agricultural University, 2019. DOI: 10.27025/d.cnki.ggsnu.2019.000134 (in Chinese)

[13] Shang L L. Research on the interaction between high-powered tractor tyres and soil. Anhui Agricultural University, 2022. DOI: 10.26919/d.cnki.gannu.2022.000760 (in Chinese)

[14] Huang K. Numerical simulation of the interaction between tractor tyres and soft ground. Jilin University, 2021. DOI: 10.27162/d.cnki.gjlin.2021.005385 (in Chinese)

[15] Yang T. Analysis of the interaction between elastic wheels and soft ground based on the discrete element method. Jilin University, 2021. DOI: 10.27162/d.cnki.gjlin.2021.005382 (in Chinese)

[16] Wang W, Zhao J F, Shen C H, Zhang X L. Design and experiment of integrated test system for terramechanics parameters. Transactions of the CSAM, 2017; 48(5): 72–78.

[17] Bekker M G. Cross-country mobility. Ordnance, 1957; 42(223): 54–56.

[18] Bernstein R. Problems with experimental engine plough mechanics. The Motor Car, 1913; 16(9): 199–206.

[19] Wang X L, Bai M Y, He J, Zhang X C, Liu K H, Liu L, et al. Laboratory assessment of the effects of straw mulch on soil compaction under static and dynamic loads. Int J Agric & Biol Eng, 2025; 18(2): 21–26.

[20] Grünberg J, Holzleitner F, Behringer M, Gollob C, Kanzian C, Katzensteiner, et al. Impacts of a fully mechanized timber harvesting system on soil physical properties after a pronounced dry period. Soil & Tillage Research, 2025; 251: 106551.

[21] Yang X, Zhai Z Q, Guo W J, Li W J, Yang M L, Song Z H. Analysis of black soil compaction with driver-agricultural machinery-soil system under corn sowing with high-power tractor in Northeast China. Int J Agric & Bio Eng, 2023; 16(4): 168–173.

[22] Thomas K. A model for the prediction of the contact area and the distribution of vertical stress below agricultural tyres from readily available tyre parameters. Biosystems Engineering, 2005; 92(1): 161–165.

[23] Castioni Guilherme A F, Lima R P, Cherubin M R, Bordonal R O, Rolim Mario M, Carvalho João L N. Machinery traffic in sugarcane straw removal operation: Stress transmitted and soil compaction. Soil & Tillage Research, 2021; 213: 105–122.

[24] Obour P B, Ugarte C M. A meta-analysis of the impact of traffic-induced compaction on soil physical properties and grain yield. Soil & Tillage Research, 2021; 211: 105019.

[25] Faloye O T, Ajayi A E, Zink A, Fleige H, Dörner J, Horn R. Effective stress and pore water dynamics in unsaturated soils: Influence of soil compaction history and soil properties. Soil & Tillage Research, 2021; 211: 104997

[26] He T F, Ding Q S, Zhang W, Jiang C X, Liu E. Optimization of analytical model based on stress transfer coefficient and soil compaction stress prediction. Transactions of the CSAM, 2020; 51(10): 292–298.

[27] He T F, Cong W J, Belal E A, Ding Q S, Yang Y S, Huo L F. Study on soil stress transfer coefficient based on compaction analysis model. Transactions of the CSAM, 2017; 48(6): 59–65.

[28] Wang X L, Zhong X K, Geng Y L, Wei Z C, Hu H, Geng D Y, et al. Calibration of no-till soil parameters based on a discrete element nonlinear elastoplastic contact model. Transactions of the CSAE, 2021; 37(23): 100–107.

[29] Zhong X K, Zhang X C, Geng Y L, Wei Z C, Chen X P, Wang X L, et al. Study on load transfer of straw-soil complex based on discrete elements. Agricultural Mechanization Research, 2023; 45(3): 17–24.

[30] Liu C Q. Study on design and control method of electro-hydraulic hitch system for high power tractor. China Agricultural University, 2021. (in Chinese)

[31] Zhang S. Study on slip rate control of heavy tractor for ploughing based on sliding mode variable structure control. China Agricultural University, 2022. (in Chinese)